Journal of Materials Chemistry A

Accepted Manuscript

ROYAL SOCIETY OF CHEMISTRY

www.rsc.org/materialsA

Table of Contents Entry

This work found out that energetic microenvironment controls the separation performance of few-layered 2D-COF membranes for CO_2 capture.

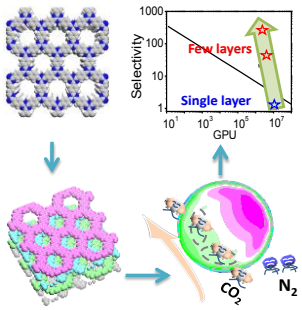

Journal Name

Few-Layered Ultrathin Covalent Organic Framework Membranes for Gas Separation: A Computational Study

Received 00th January 20xx,
Accepted 00th January 20xx

DOI: 10.1039/x0xx00000x

www.rsc.org/

Minman Tong, Qingyuan Yang*, Qintian Ma, Dahuan Liu and Chongli Zhong*

Ultrathin films have the intrinsic feature to show high flux, which may become ideal membranes if they are fabricated to also have high selectivity. 2D covalent organic frameworks (COFs) are a class of crystalline materials with well-defined layered porous structures. Utilizing this feature, 2D-COF nanosheets can be stacked into few-layered ultrathin membranes, and thus the newly formed interlayer flow passages can be regulated to tune their separation properties, making them potential candidates for high-performance membranes. In this work, a series of few-layered 2D-COF membranes were constructed to explore their capability for gas separation as well as the underlying gas transport mechanisms by taking CO_2/N_2 separation as an example. The results showed that various few-layered 2D-COF membranes can be fabricated to show very different separation performance, from nonselective to highly selective, and even to molecular sieving level. Furthermore, it was revealed that the energetic microenvironment around the narrow interlayer passages plays a crucial role, and bringing in surfaces interacted van der Waals potential sites near these passages by tuning stacking modes can achieve few-layered membranes with both high CO_2 flux and high CO_2/N_2 selectivity, leading to their separation performance far above the Robeson's upper bound. The mechanisms revealed and the design strategies proposed in this work may provide a useful guidance for preparing ultrathin membranes with outstanding performance for gas separation.

Introduction

Membrane separation technology has been considered as a promising and attractive approach for gas separation.[1] However, development of membranes with both high selectivity and high flux is still a challenge in the fields of materials, chemistry and separation.[2] It has been demonstrated that ultrathin membranes may be employed to overcome the permeability/selectivity trade-off issue, usually encountered by traditional ones such as polymeric membranes.[3-6] For this purpose, various materials have been tried to enrich the family of ultrathin membranes.[7-10] Particularly, since the successful isolation of free-standing graphene sheets in 2004,[11] great experimental[2,12,13] and computational[14-19] efforts have been devoted to exploring the gas separation performance of graphene-based membranes by artificially drilling holes on the nonporous sheets or stacking the defective sheets. Nevertheless, creating nanoholes on the sheets with precisely controlled size and desirable spatial distribution is of great challenge, and there usually is a stability problem of single-layered membranes upon external perturbations such as pressure.[20] In the meantime, although the few-layered membranes stacked by defective sheets could exhibit good separation performance, the accurately controlling the properties of the defects may be hard to realize.[21] Thus, seeking few-layered membranes with well-ordered pore structures is more favored from practical considerations.

Two-dimensional (2D) covalent organic frameworks (COFs) represent a novel class of crystalline nanoporous materials with highly-ordered honeycomb networks.[22-25] The covalently bound framework of 2D-COFs is restricted to 2D sheets which are stacked together *via* van der Waals forces to form a laminar structure.[26,27] Currently, surface-mediated synthesis method has been used to grow 2D-COF films with a single- or few-layered structure on various substrates.[28,29] Some experimental studies have also successfully shown that the bulk structures of 2D-COFs can be exfoliated into ultrathin nanosheets.[30-32] These breakthrough advances open up an exciting opportunity to find various potential applications of 2D-COF ultrathin membranes including gas separation. Since the well-defined pores of 2D-COFs can be used directly without the need of drilling holes on the nanosheets, the controllability and reproducibility of their membranes may be relatively easier to realize compared with the graphene-based ones, providing a feasible way to prepare ultrathin membranes. Nevertheless, to the best of our knowledge, the study on exploring the potential of few-layered 2D-COF ultrathin membranes for gas separation has not been reported so far.

Motivated by the above fact, a computational study was performed in this work to explore the gas separation capability of 2D-COF ultrathin membranes. For this target, a typical representative of 2D-COFs, CTF-1,[33] was chosen as a model material. A gas mixture of CO_2 and N_2 was considered as the model system to be separated. The emphasis was paid to investigate the underlying transport mechanisms that control the membrane separation performance. On the basis of the

State Key Laboratory of Organic-Inorganic Composites, Beijing University of Chemical Technology, Beijing 100029, China
E-mail: qyyang@mail.buct.edu.cn; zhongcl@mail.buct.edu.cn

† Electronic Supplementary Information (ESI) available: membrane models, probability density distributions, channel structures of the periodically-stacked few-layered membranes, CO_2 and N_2 loadings in the membranes, COM probability distributions of N_2 and the stacking environments of the local pores. See DOI: 10.1039/x0xx00000x

structure-property relationships established, some design strategies were further proposed to guide how to construct such membranes with outstanding separation performance.

Models and Computational Details

Membrane models

The layered CTF-1 membrane models were constructed using rectangular nanosheets with dimensions of 72.9 × 75.7 Å^2 and placed parallel to the *xy* plane in the center of the simulation box and the heights of both the feed and permeate sides were kept at 100 Å, as shown in Fig. S1 (see ESI†). The total height of the membrane models along z direction will be changed when stacking different number of nanosheets. A wall composed of 756 helium atoms was used at the bottom of the permeate phase to avoid molecules passing to the feed phase due to the periodicity of the simulation along the *z* axis.

Interatomic potentials

In the present study, CO_2 was modelled as a rigid linear molecule with three charged Lennard-Jones (LJ) sites locate on each atom. The potential parameters were taken from the EPM2 force field,[34] which has been proved to give good accuracy of the vapor-liquid phase equilibrium of CO_2. N_2 molecule was represented as a three-site model with two sites located at two N atoms and the third one located at its COM. The potential parameters were taken from the TraPPE force field which was developed to reproduce the experimental vapor-liquid coexistence curve and the critical properties of N_2.[35] For the interactions between the adsorbates and CTF-1, a combination of the LJ and Coulombic potentials was employed. The LJ potential parameters for the framework atoms were taken from the Dreiding force field[36] that has been widely used in the studies of MOF/COF materials,[37-39] and the partial charges were taken from our previous work.[40] The above set of force fields has been successfully used to investigate the adsorption and diffusion behaviors of CO_2, N_2 and their mixture in a wide range of MOFs[18,41,42] and COFs.[40]

Molecular dynamics simulations

The transport behaviors of CO_2/N_2 mixture through CTF-1 ultrathin membranes were studied by molecular dynamics (MD) simulations in the NVT ensemble. To obtain better statistics from MD simulations, the feed region in each system was filled up with an equimolar CO_2/N_2 mixture with the molecules randomly distributed, and this region initially contains a total of 136 molecules which corresponds to the bulk density of the mixture at 10 bar. The region underneath the membrane (that is, permeate phase) was initially empty. To mimic practical constant-pressure-gradient separation processes, molecules that pass to the permeate phase were removed every 50 ps, and certain number of molecules were added to the feed side according to the same initial composition. At the same time, the number of molecules that pass to the permeate phase were monitored against time for a total simulation time of 20 ns (40 ns in some cases). Nosé-Hoover thermostat was used to maintain the constant temperature condition. The velocity Verlet algorithm was used to integrate the Newton equations and the QUATERNION algorithm was applied for the rotational motion of CO_2 and N_2 molecules. The long-range Coulombic interactions were evaluated by the Ewald summation method, while all the LJ interactions were calculated with a cutoff radius of 14.0 Å. The time step used in the MD simulations was taken as 1.0 fs. Periodic boundary conditions were applied in the three directions. A very weak interaction was assigned between the adsorbates and He atoms to guarantee no influence on the results.[43] During the simulations, the structures of the membranes were treated as rigid. All the MD simulations were performed at 300 K using the DL_POLY program[44] with a modification. The above simulation method has been successfully used to study the performance of thin MOF membranes for CO_2/N_2 separation.[45]

Determination of molecules successfully passing the membranes

As described by Sun *et al.*,[46] gas molecules will be adsorbed onto the membrane surfaces to form adsorbed layers due to strong interactions. Thus, both the feed and permeate regions can be further divided into bulk and adsorption-layer zones. A molecule was considered to have successfully passed the membrane if it moves from the bulk zone of the feed phase to the bulk zone of the permeate phase. To determine the adsorption-layer zones, we plotted the distributions of CO_2 and N_2 molecules from the MD-simulated trajectories as a function of the distance from the membranes (see Fig. S2). The region within the two blue dotted lines is the membrane zone. It can be found that within a distance of about 6 Å from the membrane surfaces (the regions defined by the two green dotted lines), both CO_2 and N_2 form strong adsorption layers and thus these regions were considered as the adsorption-layer zone in this work. According to the method of Sun *et al*., the molecules outside of the adsorption-layer zone of the permeate phase were considered successfully passing the membranes and only these molecules were removed from the permeate phase during our simulations.

In our study, the permeances of gases were calculated using

$$P_i = \frac{F_i}{\Delta p \times A} \quad (1)$$

where P_i and F_i are the permance and molar flux of component *i*, respectively, Δp is the total pressure drop across the membrane, and A is the surface area of the membrane. The membrane selectivity ($S_{i/j}$) for component *i* over *j* was defined as the ratio of the permeances of the two components normalized by the feed composition of the mixture:

$$S_{i/j} = \frac{P_i}{P_j} \times \frac{c_j}{c_i} \quad (2)$$

where c_i is the concentration of component *i* at the upstream face of the membrane.

Calculation of potential energy distributions

A simple Monte Carlo technique was used to calculate the 2D potential energy distributions in the layers of the membranes. Specifically, one pore of the CTF-1 sheets was divided into 20 circles and then the potential energies were scanned at an

interval of two degree along the circumference of each circle. At each scanning point, 10^5 random orientations were generated for both CO_2 and N_2 molecules to obtain the lowest potential energies.

Results and Discussion

Separation performance of the CTF-1 ultrathin membranes

CTF-1 is a triazine-based 2D-COF that has an eclipsed structure with hexagonally aligned one-dimensional pores (see Fig. 1a). As a first step, MD simulation was conducted to examine the separation properties of the one-atom-thick single-layered CTF-1 membrane. The results show that the membrane can exhibit a permeance for both gases on the order of 10^7 GPU (gas permeation unit, 1 GPU = 3.35×10^{-10} mol m^{-2} s^{-1} Pa^{-1}) but with a poor CO_2/N_2 selectivity (~0.89). This is not unexpected since the pore size of CTF-1 (12 Å) is much larger than the kinetic diameters of both CO_2 and N_2 molecules (3.3 and 3.68 Å, respectively), leading to a typical Knudsen transport of gases through the membrane.

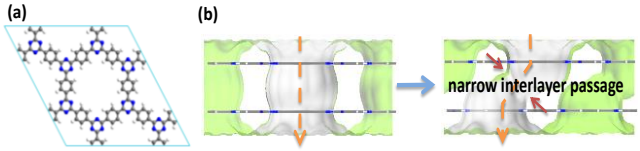

Fig. 1 a) Crystalline structure of CTF-1 viewed along the *z* direction (C, gray; N, blue; H, white). b) Illustration of the variation of the flow channels in the CTF-1 membranes with perfectly- and imperfectly-overlapped layers.

If the one-atom-thick CTF-1 nanosheets are stacked in a mode different from the perfectly-overlapped one in the bulk structure, narrow interlayer passages will be formed between adjacent layers and controllable flow channels will be generated in the layered membranes (Fig. 1b). To conveniently show the influence of the narrow interlayer passages on the transport of gases, a series of two-layered CTF-1 membranes with different sizes of such passage were constructed by shifting their relative positions as shown in Fig. 2a, where the angle formed by the ABC atoms (blue) was fixed when shifting the layers, and only the distance between the BC atoms (blue) was tuned. Fig. 2b presents a relationship between the MD-simulated CO_2/N_2 selectivities and CO_2 permeances of the five so-built membranes. It can be found the selectivities of pore-1 to pore-4 membranes can increase from 7 to 190, in line with the size-decreasing sequence of their narrow interlayer passages. Compared with the single-layered membrane, this figure shows that the selectivity can be greatly enhanced by rationally stacking the layers, together with the CO_2 permeances still remaining on the order of magnitude of ~10^6 GPU. Our simulation results also found that the two-layered membrane with the nanosheets overlapped perfectly exhibit a similar separation performance to the single-layered one. In addition, the MD-simulated trajectories show that only two and no N_2 molecules can pass through the pore-4 and pore-5 membranes respectively even when extending the simulation time to 40 ns. These observations demonstrate that the narrow interlayer passages formed in the membranes can act as a "gate" to exert a so-called "gate-closing" effect on the selective transport of molecules. By tuning the size of these passages, it will lead to the membrane performance from nonselective to highly selective, and even to molecular sieving level.

It has been claimed that 2D-sheet stacked ultrathin membranes with molecular sieving properties are industrially attractive candidates for gas separations.[47,48] However, certain difficulties perhaps exist in achieving such nanostructured membranes with ideal transport pore sizes for gases. From practical point of view, depositing more sheets may be considered as an alternative to prepare ultrathin membranes. Therefore, there currently is an increasing demand to understand the separation mechanisms of few-layered nanoporous membranes beyond the scope of molecular sieving.[48] For this purpose, the two-layered pore-1 membrane built previously with a low selectivity was chosen to construct few-layered membranes for further investigations. In light of experimental observations on the structures of some few-layered 2D-COFs[30,31] as well as the few-layer stacked graphene membranes,[2] the interlayer distance in all the designed membranes was kept the same as that in the bulk structure of CTF-1 (3.4 Å).

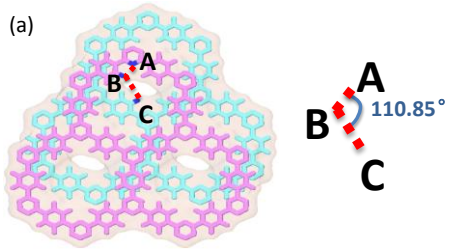

Pore No.	BC distance (Å)
1	5.81
2	5.68
3	5.42
4	5.23
5	5.08

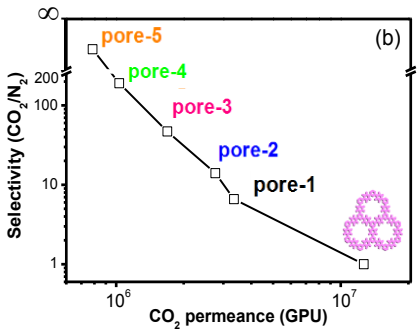

Fig. 2 a) Structural features of the five CTF-1 membranes stacked from two one-atom-thick layers, where the shadow region in the structure represents the impermeable surface for the gases, while the white areas are the newly generated narrow interlayer passages. b) The CO_2 permeances and CO_2/N_2 selectivities of the five membranes together with those of the single-layered one.

Starting from the pristine structure of this membrane, a series of few-layered membranes were designed by keeping the shape and size of the narrow interlayer passages unchanged. One advantage of such treatment is that the influencing factors can be reduced when exploring the

transport mechanisms in the designed ultrathin membranes. Initially, the thickness of the membranes was "periodically" increased to contain 3 or 4 layers of the CTF-1 framework (see Fig. S3). Compared with the pristine pore-1 membrane, the simulation results show that there are 50%~65% decreases in the permeance of CO_2 through the two designed membranes, while the CO_2/N_2 selectivity is only slightly improved from about 7 to 10 and 11, respectively.

To examine whether more selective ultrathin membranes can be achieved, the structure of the four-layered membrane was further changed by altering the stacking modes among the one-atom-thick nanosheets. Specifically, by fixing the positions of the 1st and 2nd layers in the periodically stacked membrane (denoted as No. 6), the 3rd and 4th layers were shifted but with the size of the narrow interlayer passage remaining unchanged. Fig. 3 shows the channel structures of the five so-obtained membranes (No. 1 to 5). Obviously, the flow channels in these four-layered membranes have different orientations and these channels consist of alternate wide pores and narrow interlayer passages. This figure also shows that the newly constructed membranes, excepting the No. 5, exhibit much better separation performance compared with the original pore-1, and the membranes with higher CO_2 flux are generally more selective. Interestingly, it seems that there is no clear relationship between the separation performance and the shape of the flow channels, e.g., the CO_2 fluxes of the No. 2 and 3 membranes with tortuous channels are higher than that of the No. 5 membrane with a straight-like one.

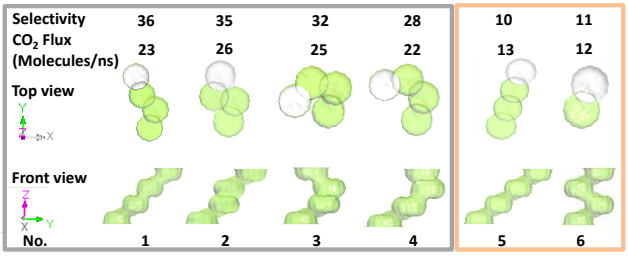

Fig. 3 Channel structures of the six four-layered CTF-1 membranes and the corresponding CO_2 fluxes and CO_2/N_2 selectivities. In the top view, the region with silver-grey color is the channel of the fourth layer in each membrane. In the front view, the channels from bottom to up are the first to the fourth layers with the first layer located at the feed side during the simulations.

Fig. 4 shows a comparison of the CO_2/N_2 separation performance of the designed two- and four-layered CTF-1 membranes with some typical polymeric, inorganic, MOF and their composite membranes reported in the literature. It can be found that the CTF-1 ultrathin membranes are highly permeable for CO_2 and their separation performance can exceed the Robeson's upper bound. Moreover, due to a good combination of the CO_2/N_2 selectivity and the CO_2 permeance, their separation performances can be regarded superior to other membranes. In addition, according to the suggestion of Merkel *et al.*,[49] membranes with a selectivity larger than 30 and a CO_2 permeance above 4000 GPU could offer a capture cost below \$17/ton CO_2, which is lower than the DOE target goal of \$20/ton CO_2.[50] This figure indicates that the rationally designed ultrathin membranes of 2D-COFs could be considered as an energy-saving alternative for CO_2 capture.

As water is usually present in flue gas, it would be worthy of studying the effect of humidity on the performance of the membranes for CO_2/N_2 separation. Considering this, we performed some additional MD simulations to preliminarily study the effect of trace amount of water by taking the four-layered membrane No. 1 with good separation performance for the dry mixture as an example. The molar content of H_2O in the feed mixture was varied up to 7%. As shown in Fig. S4 (see ESI†), there is almost no influence on the separation performance of this membrane within the examined range of the water content, both in the CO_2/N_2 selectivity and the CO_2 permeance.

Transport mechanisms in the few-layered ultrathin membranes

In light of the good separation performance of the designed few-layered membranes, it is necessary to give deep insight into the microscopic transport mechanisms related to the preceding observations. This is not only fundamentally interesting but will also be beneficial to further enhance the CO_2/N_2 separation performance of membranes. Fig. S5 shows the statistically-averaged loadings of CO_2 and N_2 molecules in the six designed membranes. One can observe that there is a similar amount of CO_2 (or N_2) resided in these four-layered membranes and CO_2 exhibits a loading about ten times larger than that of N_2. This means that the membranes have a much stronger adsorption affinity toward CO_2, resulting in their pores mainly occupied by CO_2 molecules. Therefore, the following mechanism analyses were mainly focused on this component.

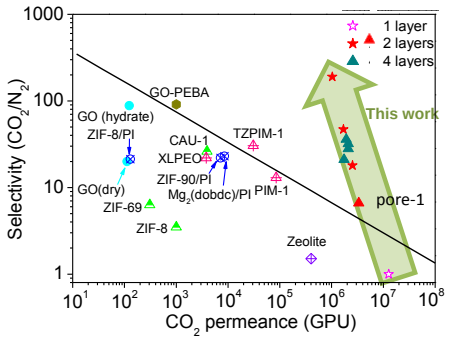

Fig. 4 Comparison of gas separation performance between few-layered CTF-1 membranes and some typical membranes reported in the literature.[2,51-58] The black solid line represents the Robeson's 2008 upper bound[59] of polymeric membranes for CO_2/N_2 separation. The four-layered membranes are designed from the two-layered pore-1. For other membranes used for comparison, a thickness of 0.1 μm is used in the conversion if their CO_2 permeances are not given in unit of GPU in the corresponding studies.

Fig. 5a shows the calculated center of mass (COM) probability distributions of CO_2 molecules in the six membranes. Obviously, CO_2 molecules can accumulate inside the pores of each layer but the densities in the 2nd and 3rd layers are much higher compared with those in the 1st and 4th layers. The diffusion paths of CO_2 molecules (denoted by the orange dashed lines) indicate that the six membranes share a

common feature: gas molecules have to diffuse along the narrow interlayer passages and exhibit a jump behavior from the inlets in one layer to the outlets in the adjacent layer. For the No. 5 and 6 membranes, CO_2 molecules show very strong local distributions in the pores of the 2nd and 3rd layers but are weakly distributed near the inlets and outlets for interlayer transfer. In contrast, for the No. 1 to 4 membranes, CO_2 molecules exhibit more even and wider distribution in these regions. For the case of N_2, besides the much weaker densities in the six membranes compared with those of CO_2, molecules also distribute more evenly in the No. 5 and 6 membranes (see Fig. S6, ESI†). Due to the same size of the narrow interlayer passages, it may be speculated from these analyses that unfavorable energetic microenvironment should exist in the No. 5 and 6 membranes, which results in the hard escape of CO_2 from the attractive low-energy regions to the diffusion ports. It will in turn facilitate the transport of N_2 through the membranes and thus lead to both low CO_2 flux and CO_2/N_2 selectivity.

To validate the above speculation, Fig. 5b and c show the 2D potential energy maps calculated for CO_2 in the pores of the 2nd and 3rd layers, respectively. For each layer of the periodically-stacked membrane (No. 6), the interlayer diffusion ports are located in the heavy green high-energy regions (less negative values) and the energies around these ports drop significantly with a gradient of about 9.5 kJ/mol. This unfavorable energetic microenvironment plays a role like steep sliding ladder to cause that CO_2 molecules are tightly captured in the magenta low-energy regions; this finally gives rise to a low CO_2 flux of the membrane although the inlets and outlets for interlayer diffusion are overlapped. For the No. 5 membrane, the diffusion ports are situated in the white energy

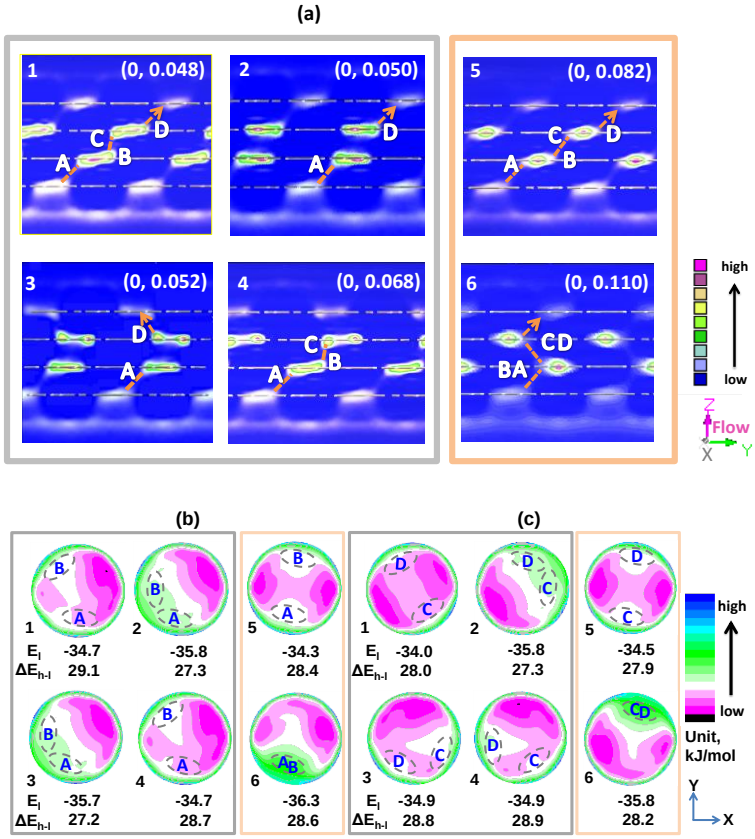

Fig. 5 a) Contour plots of the COM probability distributions of CO_2 in the six designed membranes, where the orange dashed lines represent the CO_2 diffusion paths between the layers observed from the *x* direction. One path for the No. 2 to 4 membranes is not shown because of the need to observe from the *y* axis. The two values in the bracket given in each subfigure represent the lowest and the highest number densities in the distributions. b and c) Contour plots of the 2D potential energy distributions for CO_2 in the pores of the 2nd (b) and 3rd (c) layers of the six membranes. The two numbers (units: kJ/mol) under each map represent the values of the lowest potential energy (E_i, the most negative one) and the difference between the highest and lowest energies ($\Delta E_{h\text{-}l}$). A denotes the outlet of the narrow interlayer passage between the 1st and 2nd layers, B denotes the inlet of that between the 2nd and 3rd layers, C denotes the outlet of that between the 2nd and 3rd layers, and D denotes the inlet of that between the 3rd and 4th layers.

regions in the pores. Because of a need to cross the much more attractive magenta area, there is a relatively large barrier for CO_2 molecules when diffusing from the outlets to the opposite inlets. Such an obstacle leads to a poor separation performance of the membrane. For the other four membranes, the easy diffusion of CO_2 molecules can be explained from two aspects. One is that some diffusion ports are located in the low-energy regions (see the No. 1 and No. 4 membranes); in this case, CO_2 can be favorably adsorbed around the diffusion ports and thus increase the transport probability of CO_2 between the layers. The other is that the diffusion inlets and outlets are closely located in the regions with a relatively low and smooth energy platform, as can be observed for the No. 2 and 3 membranes; in this case, certain portion of CO_2

molecules can be adsorbed here and the closely located diffusion ports can also reduce the residence time of CO_2 in the pores. Such distinctive microenvironments in the four membranes can benefit the interlayer transport of CO_2, making them much better separation performance compared with the No. 5 and 6 membranes. Because the CO_2 fluxes shown in Fig. 3 obtained statistically reflect how difficult the transport of CO_2 molecules through the membranes, these data can be further used to support the above discussion of CO_2 interlayer movement.

From the above analyses, it can be concluded that the transport rate of CO_2 passing the narrow interlayer passages is the bottleneck that affects the separation performance of the few-layered 2D-COF membranes. The transport rate can be greatly influenced by the energetic microenvironment around the diffusion ports of the interlayer narrow passages, where the occurrence of low and smooth potential energy platform can effectively facilitate the permeance of CO_2 through the membranes and also will induce an enhancement on the CO_2/N_2 selectivity.

Design strategy for few-layered ultrathin membranes

To guide the structural design of few-layered ultrathin membranes, a respective single pore in the 2nd and 3rd layers of the membranes with the up-down stacking environments by the adjacent layers was further selected to study (see Fig. S7, ESI†). For simplicity, the analysis was firstly performed on the structure of the No. 6 membrane with periodically stacked nanosheets in which the 1st (or 2nd) and the 3rd (or 4th) layers are exactly overlapped. Fig. 6a shows a perspective view of the local configuration of the pore in the 2nd layer. The area enclosed by the black dashed line approximately represents the low-energy region in the corresponding map shown in Fig. 5b. It can be found that there is a high planar projection density of the atoms from the three layers in the enclosed area. However, the diffusion ports are situated in the open area (the region enclosed by the gray dashed line) in lack of interacting surfaces which correspond to the heavy green high-energy regions shown in Fig. 5b, and thus the weak interactions lead to few CO_2 molecules that can reside here.

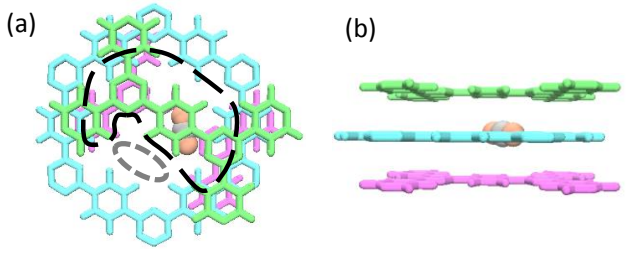

Fig. 6 a) Perspective top view of a single pore in the 2nd layer of the No. 6 membrane with the up-down stacking environments by the adjacent layers, where the area enclosed by the black dashed line approximately represents the low-energy region in the corresponding map shown in Fig. 5b, while the area enclosed by the gray dashed line is the region located by the diffusion ports. b) Front view of this local structure with an adsorbed CO_2 molecule. (1st layer, pink; 2nd layer, aquamarine; 3rd layer, green; CO_2: C, silver; O, yolk yellow)

When turning to the local configurations of the other five membranes, we found that the higher density the atoms of the three layers (1st-2nd-3rd or 2nd-3rd-4th) emerging simultaneously on the planar projection, the lower the CO_2 potential energy in the corresponding region is. Thus, the lowest-energy regions are always located near the edges of the pores where the highest atomic densities occur, as shown in Fig. 5b and c. This common feature indicates that the existence of "surface" would lead to a more attractive microenvironment for molecules. Essentially, such "surface" can provide van der Waals-type interaction sites for molecules, and thus multiple "surfaces" composed of the sandwich layers and the pore walls would lead to a strong adsorption affinity for CO_2 (Fig. 6b). For the No. 1 to No. 4 membranes, the "surfaces" of the adjacent layers appear around the diffusion ports, which form a favorable energetic microenvironment for CO_2 to cross the interlayer narrow passage. In contrast, for the No. 5 membrane, although the "surfaces" also appear around the diffusion ports, they cannot provide sufficient driving force when the molecules cross the area with lower potential energy to arrive the other diffusion port (Fig. 5b and c). Consequently, it may be concluded that the energetic microenvironment plays a crucial role in the separation performance of few-layered membranes. In the design and preparation of few-layered 2D-COF membranes, tuning the stacking modes to introduce surface-interacted van der Waals potential sites near the narrow interlayer passage is an effective approach to increase the transport probability of CO_2 through the membranes. On the basis of such favorable energetic microenvironment, close diffusion ports in the same layers will also be beneficial to achieve ultrathin membranes with both high flux and selectivity.

Conclusions

In conclusion, 2D-COFs with well-ordered pore structure can act as an ideal platform to fabricate ultrathin membranes by stacking their one-atom-thick nanosheets. With a triazine-based material CTF-1 as a representative of 2D-COFs, a systematic study was performed to investigate the performance of a series of designed few-layered ultrathin membranes for CO_2/N_2 separation. The foregoing results demonstrate that that the narrow interlayer passages formed between the stacked nanosheets can exert a "gate-closing" effect on the selective transport of molecules. Regulating the size of these passages can lead to various few-layered 2D-COF membranes with very different separation performance, from nonselective to highly selective, and even to molecular sieving level. Furthermore, tuning the stacking modes of the nanosheets to construct a favorable energetic microenvironment can be considered as an effective regulation and control strategy for achieving few-layered ultrathin membranes with both high flux and high selectivity. Such energetic microenvironments can be accomplished by introducing surface interacted van der Waals potential sites near the narrow interlayer passages. It could be expected that the information obtained in this work not only will facilitate

the use of 2D-COFs as precursor materials to prepare ultrathin membranes for gas separation applications, but also will enrich the knowledge of understanding the transport behavior of gases in many other layer-stacked membranes.

Acknowledgements

The authors would like to thank Prof. Perla B. Balbuena from Texas A&M University for her warm help in computation methods. This work was supported by the National Key Basic Research Program of China ("973") (2013CB733503) and Natural Science Foundation of China (Nos. 21136001 and 21322603).

References

1 A. Brunetti, F. Scura, G. Barbieri and E. Drioli, *J. Membr. Sci.*, 2010, **359**, 115-125.
2 H. W. Kim, H. W. Yoon, S.-M. Yoon, B. M. Yoo, B. K. Ahn, Y. H. Cho, H. J. Shin, H. Yang, U. Paik, S. Kwon, J.-Y. Choi and H. B. Park, *Science*, 2013, **342**, 91-95.
3 Z. Lai, G. Bonilla, I. Diaz, J. G. Nery, K. Sujaoti, M. A. Amat, E. Kokkoli, O. Terasaki, R. W. Thompson, M. Tsapatsis and G. Dionisios, *Science*, 2003, **191**, 456-460.
4 S. Keskin and D. S. Sholl, *Energy Environ. Sci.*, 2010, **3**, 343-351.
5 T. Ohba, *ACS Nano*, 2014, **8**, 11313-11319.
6 D. Wu, G. Maurin, Q. Yang, C. Serre, H. Jobic and C. Zhong, *J. Mater. Chem. A*, 2014, **2**, 1657-1661.
7 K. Varoon, X. Zhang, B. Elyassi, D. D. Brewer, M. Gettel, S. Kumar, J. A. Lee, S. Maheshwari, A. Mittal, C.-Y. Sung, M. Cococcioni, L. F. Francis, A. V. McCormick, K. A. Mkhoyan and M. Tsapatsis, *Science*, 2011, **334**, 72-75.
8 P. Kumar, K. V. Agrawal, M. Tsapatsis and K. A. Mkhoyan, *Nat. Commun.*, 2015, **6**, 7128.
9 Y. Peng, Y. Li, Y. Ban, H. Jin, W. Jiao, X. Liu and W. Yang, *Science*, 2014, **346**, 1356-1359.
10 B. A. Al-Maythalony, O. Shekhah, R. Swaidan, Y. Belmabkhout, I. Pinnau and M. Eddaoudi, *J. Am. Chem. Soc.*, 2015, **137**, 1754-1757.
11 K. S. Novoselov, A. K. Geim, S. V. Morozov, D. Jiang, Y. Zhang, S. V. Dubonos, I. V. Grigorieva and A. Firsov, *Science*, 2004, **306**, 666-669.
12 S. P. Koenig, L. Wang, J. Pellegrino and J. S. Bunch, *Nat. Nanotechnol.*, 2012, **7**, 728-732.
13 H. Li, Z. Song, X. Zhang, Y. Huang, S. Li, Y. Mao, H. J. Ploehn, Y. Bao and M. Yu, *Science*, 2013, **342**, 95-98.
14 D. Jiang, V. R. Cooper and S. Dai, *Nano Lett.*, 2009, **9**, 4019-4024.
15 J. Schrier, *J. Phys. Chem. Lett.*, 2010, **1**, 2284-2287.
16 T. Wu, Q. Xue, C. Ling, M. Shan, Z. Liu, Y. Tao and X. Li, *J. Phys. Chem. C*, 2014, **118**, 7369-7376.
17 L. W. Drahushuk and M. S. Strano, *Langmuir*, 2012, **28**, 16671-16678.
18 Q. Yang, D. Liu, C. Zhong and J.-R. Li, *Chem. Rev.*, 2013, **113**, 8261-8323.
19 D. Liu and C. Zhong, *J. Mater. Chem.,* 2010, **20**, 10308-10318.
20 S. Jiao and Z. Xu, *ACS Appl. Mater. Interfaces*, 2015, **7**, 9052-9059.
21 F. Banhart, J. Kotakoski and A. V. Krasheninnikov, *ACS Nano*, 2011, **5**, 26-41.
22 A. P. Côté, A. I. Benin, N. W. Ockwig, M. O'Keeffe, A. J. Matzger and O. M. Yaghi, *Science*, 2005, **310**, 1166-1170.
23 J. L. Mendoza-Cortes, T. A. Pascal and W. A. Goddard III, *J. Phys. Chem. A*, 2011, **115**, 13852-13857.
24 R. L. Martin, C. M. Simon, B. Smit and M. Haranczyk, *J. Am. Chem. Soc.*, 2014, **136**, 5006-5022.
25 E. Klontzas, E. Tylianakis and G. E. Froudakis, *Nano Lett.*, 2010, **10**, 452-454.
26 D. D. Medina, V. Werner, F. Auras, R. Tautz, M. Dogru, J. Schuster, S. Linke, M. Döblinger, J. Feldmann, P. Knochel and T. Bein, *ACS Nano*, 2014, **8**, 4042-4052.
27 R. Babarao and J. Jiang, *Energy Environ. Sci.*, 2008, **1**, 139-143.
28 J. W. Colson, A. R. Woll, A. Mukherjee, M. P. Levendorf, E. L. Spitler, V. B. Shields, M. G. Spencer, J. Park and W. R. Dichtel, *Science*, 2011, **332**, 228-231.
29 N. A. A. Zwaneveld, R. Pawlak, M. Abel, D. Catalin, D. Gigmes, D. Bertin and L. Porte, *J. Am. Chem. Soc.*, 2008, **130**, 6678-6679.
30 I. Berlanga, M. L. Ruiz-González, J. M. González-Calbet, J. L. G. Fierro, R. Mas-Ballesté and F. Zamora, *Small*, 2011, **7**, 1207-1211.
31 S. Chandra, S. Kandambeth, B. P. Biswal, B. Lukose, S. M. Kunjir, M. Chaudhary, R. Babarao, T. Heine and R. Banerjee, *J. Am. Chem. Soc.*, 2013, **135**, 17853-17861.
32 D. N. Bunck and W. R. Dichtel, J. *Am. Chem. Soc.*, 2013, **135**, 14952-14955.
33 P. Kuhn, M. Antoniett and A. Thomas, *Angew. Chem. Int. Ed.*, 2008, **47**, 3450-3453.
34 G. Harris and K. H. Yung, *J. Phys. Chem.*, 1995. **99**, 12021-12024.
35 J. J. Potoff and J. I. Siepmann, *AIChE J.*, 2001, **47**, 1676-1682.
36 S. L. Mayo, B. D. Olafson and W. A. Goddard III, *J. Phys. Chem.*, 1990, **94**, 8897-8909.
37 D. A. Gomez, A. F. Combariza and G. Sastre, *Phys. Chem. Chem. Phys.*, 2012, **14**, 2508-2517.
38 Y. J. Colón and R. Q. Snurr, *Chem. Soc. Rev.*, 2014, **43**, 5735-5749.
39 J. A. Greathouse, T. L. Kinnibrugh and M. D. Allendorf, *Ind. Eng. Chem. Res.*, 2009, **48**, 3425-3431.
40 M. Tong, Q. Yang, Y. Xiao and C. Zhong, *Phys. Chem. Chem. Phys.*, 2014, **16**, 15189-15198.
41 J. R. Karra and K. S. Walton, *J. Phys. Chem. C*, 2014, **114**, 15735-15740.
42 R. Krishna and J. M. van Baten, *Phys. Chem. Chem. Phys.*, 2011, **13**, 10593-10616.
43 K. Yin, *Chem. Eng. Commun.*, 2006, **193**, 1678–1688.
44 W. Smith and T. R. Forester, *J. Mol. Graph.* 1996, **14**, 136-141.
45 F. A. Cabrales-Navarro, J. L. Gómez-Ballesteros and P. B. Balbuena, *J. Membr. Sci.*, 2013, **428**, 241-250.
46 C. Sun, M. S. H. Boutilier, H. Au, P. Poesio, B. Bai, R. Karnik and N. G. Hadjiconstantinou, *Langmuir*, 2014, **30**, 675-682.
47 Y. Liu, J. H. Pan, N. Wang, F. Steinbach, X. Liu and J. Caro, *Angew. Chem. Int. Ed.*, 2015, **54**, 3028-3032.
48 W. Kim and S. Nair, *Chem. Eng. Sci.*, 2013, **104**, 908-924.
49 T. C. Merkel, H. Lin, X. Wei and R. Baker, *J. Membr. Sci.*, 2010, **359**, 126-139.
50 D. Figueroa, T. Fout, S. Plasynski, H. McIlvried and R. D. Srivastava, *Int. J. Greenhouse Gas Control*, 2008, **2**, 9-20.
51 H. Yin, J. Wang, Z. Xie, J. Yang, J. Bai, J. Lu, Y. Zhang, D. Yin and J. Y. S. Lin, *Chem. Commun.*, 2014, **50**, 3699-3701.
52 Y. Liu, G. Zeng, Y. Pan and Z. Lai, *J. Membr. Sci.*, 2011, **379**, 46-51.
53 Q. Song, S. K. Nataraj, M. V. Roussenova, J. C. Tan, D. J. Hughes, W. Li, P. Bourgoin, M. A. Alam, A. K. Cheetham, S. A. Al-Muhtaseb and E. Sivaniah, *Energy Environ. Sci.*, 2012, **5**, 8359-8369
54 N. Du, H. B. Park, G. P. Robertson, M. M. Dal-Cin, T. Visser, L. Scoles and M. D. Guiver *Nat. Mater.*, 2011, **10**, 372-375.
55 M. C McCarthy, V. Varela-Guerrero, G. V. Barnett and H.-K. Jeong, *Langmuir*, 2010, **26**, 14636-14641.
56 T.-Y. Bae and J. R. Long, *Energy Environ. Sci.*, 2013, **6**, 3565-3569.

57 J. Shen, G. Liu, H. Kang, W. Jin, K.-R. Lee and N. Xu, *Angew. Chem. Int. Ed.*, 2014, **54**, 578-582.
58 T. Bae, J. S. Lee, W. Qiu, W. J. Koros, C. W. Jones and S. Nair, *Angew. Chem. Int. Ed.*, 2010, **49**, 9863-986.
59 L. M. Robeson, *J. Membr. Sci.*, 2008, **320**, 390-400.